Synthesis of Ag/Pd Nanoparticles and Their Low-Temperature Alloying within Thermally Evaporated Fatty Acid Films

Chinmay Damle, Ashavani Kumar, and Murali Sastry*

Materials Chemistry Division, National Chemical Laboratory, Pune - 411 008, India

Received: September 20, 2001

The low-temperature alloying of Ag/Pd nanoparticles synthesized in a fatty acid film by a novel ion-entrapment process is described. Nanoparticles of silver and palladium were grown in thermally evaporated fatty acid (stearic acid) films by immersion of the film sequentially in solutions containing Ag^+ ions and Pd^{2+} ions followed by their in-situ reduction at each stage. Incorporation of Ag^+ and Pd^{2+} ions into the stearic acid film occurs by selective electrostatic binding with the carboxylate ions in the fatty acid matrix. It is observed that the reduction of the Pd^{2+} ions in the stearic acid−Ag nanocomposite film leads to the formation of a mixture of individual Ag and Pd nanoparticles as well as particles in the Ag-core/Pd-shell structure. Thermal treatment of the stearic acid−(silver + palladium) nanocomposite film at 100 °C resulted in the formation of an Ag−Pd alloy. The process of Ag^+ and Pd^{2+} ion incorporation in the stearic acid matrix, their reduction to form metallic nanoparticles, and synthesis of the Ag−Pd alloy were followed by quartz crystal microgravimetry (QCM), Fourier transform infrared (FTIR) spectroscopy, transmission electron microscopy (TEM), UV−vis spectroscopy, and X-ray diffraction (XRD) measurements.

Introduction

The design, synthesis, and characterization of nanophase materials are subjects of intense research due to the exciting optoelectronic and physicochemical properties of nanoscale matter.[1] One aspect of nanotechnology where there will always be scope for experimentation is the synthesis of nanoparticles in different hosts to yield nanohybrid materials. A number of different templates such as polymers,[2] porous glasses,[3] zeolites,[4] phospholipid membranes,[5] inverse microemulsions,[6] poly(amidoamine) dendrimers,[7] self-assembled monolayers,[8] as well as biotemplates such as self-assembled bacterial S-layers[9] and the tobacco mosaic virus (TMV)[10] have been used for the synthesis of nanoparticles. Organic thin films such as Langmuir−Blodgett (LB) films have also been investigated in fair detail for the in-situ growth of metal/semiconductor/oxide nanoparticles either by chemical reaction or thermal treatment of entrapped metal ions.[11]

Bimetallic nanoparticles, in particular, are being investigated at some depth. Due to the high catalytic activity of Pd and Pt, bimetallic colloids of gold and silver in combination with Pd and Pt (Pd−Pt,[12] Ag−Pt,[13] Au−Pt,[14] and Au−Pd[15]) have been studied in great detail. Bimetallic Ag−Au[16] and Cu−Pd[17] colloids have also been synthesized and characterized using various techniques. Bimetallic Ag−Pd nanoparticles have been synthesized by UV irradiation of an oxalate precursor,[18] by heterogeneous reaction of $AgNO_3$ and PdO_x[17a] with dry methanol, and by reduction of silver ions on the surface of palladium particles.[19] Developing on our earlier work on the incorporation of metal cations in thermally evaporated lipid films,[20] we show in this paper that Ag^+ and Pd^{2+} ions may be electrostatically entrapped within thermally evaporated fatty acid (stearic acid, StA) films and that their in-situ reduction results in the formation of both Ag and Pd nanoparticles as well as particles in Ag-core/Pd-shell structure (Scheme 1). Low-temperature heat treatment at 100 °C leads to the alloying of the individual nanoparticles as well as the core−shell nanostructures and creation of a crystalline Ag_xPd_{1-x} solid solution within the lipid matrix (Scheme 1). The processes of ion entrapment, synthesis of the Ag/Pd nanoparticles, and their alloying have been studied using quartz crystal microgravimetry (QCM), UV−vis spectroscopy, Fourier transform infrared (FTIR) spectroscopy, transmission electron microscopy (TEM), and X-ray diffraction (XRD) measurements. Presented below are details of the investigation.

Experimental Details

Thin films of stearic acid (StA, 500 Å thickness) were thermally vacuum deposited in an Edwards E306 vacuum coating unit operated at a pressure of 1×10^{-7} Torr onto gold-coated AT-cut quartz crystals, quartz substrates, and Si (111) substrates for QCM, UV−vis, and FTIR spectroscopy/X-ray diffraction measurements, respectively. 500 Å thick StA films were also deposited on carbon-coated TEM grids for transmission electron microscopy measurements. The film thickness and deposition rate were monitored in situ using an Edwards thickness monitor. The kinetics of incorporation of Ag^+ ions into the stearic acid films was followed by measurement of the change in resonance frequency of the stearic acid covered QCM crystal during immersion in 10^{-4} M Ag_2SO_4 solution at pH 6. The frequency measurements were made ex-situ on an Edwards FTM5 frequency counter (stability and resolution of 1 Hz) after thorough washing of the crystals with deionized water and drying in flowing N_2. For the 6 MHz crystal used in this study, the mass resolution was 12.1 ng/cm^2 and the frequency changes were converted to mass loading using the Sauerbrey equation.[21] The optimum immersion time determined from the QCM kinetics measurements was used to load the stearic acid films on quartz, Si (111) substrates, and TEM grids with Ag^+ ions by similar immersion in 10^{-4} M Ag_2SO_4 solution. After

* To whom all correspondence is to be addressed. Ph: +91 20 5893044. Fax: +91 20 5893952/5893044. E-mail: sastry@ems.ncl.res.in.

10.1021/jp013468c CCC: $22.00
Published on Web 12/20/2001

SCHEME 1

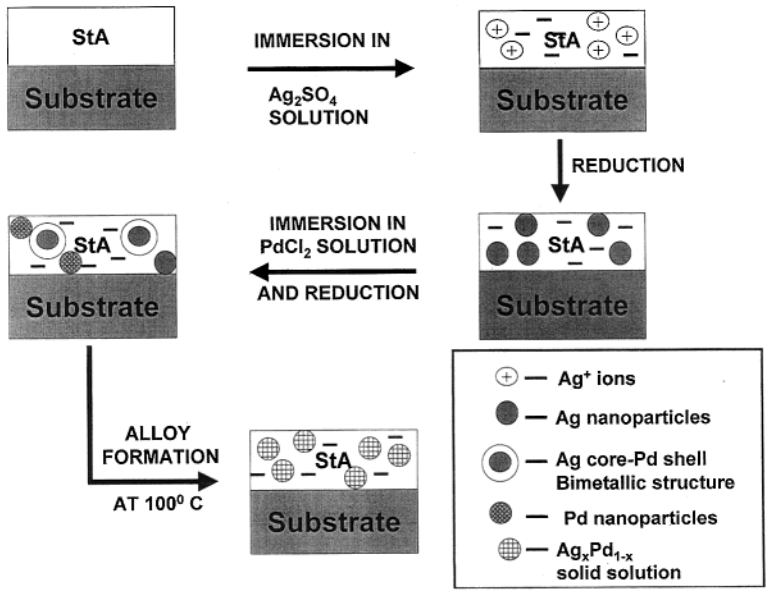

formation of silver stearate films, the films on Si (111) substrates were subjected to FTIR and XRD analysis. FTIR measurements were carried out in the diffuse reflectance mode at a resolution of 4 cm^{-1} on a Shimadzu FTIR-8201 PC instrument, while XRD studies were carried out in the transmission mode on a Philips PW 1830 instrument operating at 40 kV voltage and a current of 30 mA with Cu Kα radiation. Thereafter, the silver stearate films on the different substrates were kept in an atmosphere of hydrazine to reduce the silver ions in the lipid film. After hydrazine treatment (which required typically 2 h), it was observed that there was a small increase in the mass of the silver stearate film on the QCM crystal that was attributed to trapped hydrazine in the film. Mild heating at ca. 50 °C for 15 min resulted in removal of the trapped hydrazine and restoration of the film mass to the value measured at the start of hydrazine treatment. This mild heat treatment was given before each successive cycle of ion-exchange and reduction. It could be seen that the film on quartz acquired a deep brown color on reduction of the silver ions with hydrazine and was analyzed by UV−vis spectroscopy using a Hewlett-Packard 8542A diode array spectrophotometer operated at a resolution of 2 nm. The reduced films were also analyzed by FTIR, XRD, and TEM. TEM measurements were carried out on a JEOL Model 1200EX instrument operated at an accelerating voltage of 120 kV. The nanoparticle films for TEM analysis were prepared by immersing the TEM grids in chloroform for 15 min in order to dissolve the lipid matrix and has previously been shown to lead to close-packing of the nanoparticles.[22]

On completion of the first cycle of Ag^+ incorporation and reduction, QCM measurements of the kinetics of Pd^{2+} incorporation in the StA−Ag nanofilm were performed by immersion of the StA−Ag nanofilm in 10^{-4} M $PdCl_2$ solution (pH 6) and monitoring ex-situ the frequency changes of the quartz crystal. On completion of the Pd^{2+} ion exchange cycle, the ions were reduced with hydrazine in a manner similar to that adopted for the silver stearate film and the films on different substrates analyzed by UV−vis, FTIR, XRD, and TEM measurements. It was observed that the extent of Pd^{2+} incorporation in the films was much smaller than that of Ag^+ ions, and therefore, three cycles of Pd^{2+} exchange and reduction were required before a measurable signal from the Pd nanoparticles (the (111) Bragg reflection from Pd at a 2θ value of 40° was used an indicator)

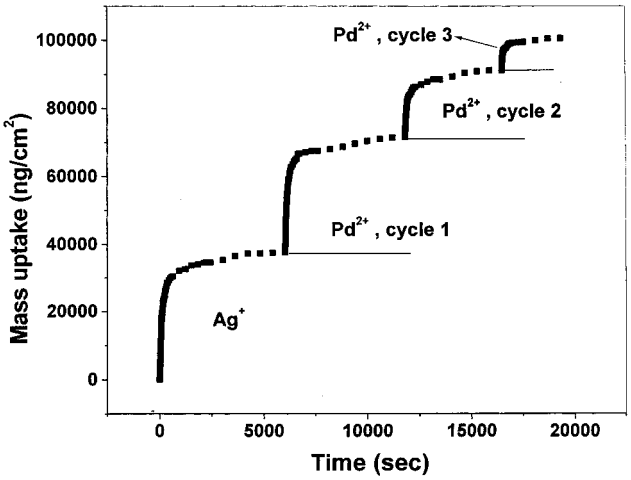

Figure 1. QCM mass uptake recorded ex-situ during Ag^+ and Pd^{2+} ion incorporation in a 50 nm thick thermally evaporated StA film (see text for details). The different cycles of ion exchange are indicated next to the respective curves.

could be observed. The size of the silver and Ag-core/Pd-shell particles in the film were estimated from an analysis of the TEM micrographs obtained from the films.

The thermal stability of the film and the formation of an Ag−Pd alloy were studied by heating the lipid−Ag/Pd nanocomposite film to different temperatures and following changes in the XRD patterns. The films were heated at 50 and 100 °C for 6 h and finally at 100 °C for 12 h.

Results and Discussion

The kinetics of incorporation of Ag^+ and Pd^{2+} ions into a 500 Å thick StA was followed by QCM, and the data obtained is shown in Figure 1. The individual cycles of mass exchange are clearly indicated in the figure next to the respective curves. The first cycle of Ag^+ incorporation into the film resulted in a mass uptake of ca. 38 000 ng/cm^2. From the mass of StA deposited onto the quartz crystal (ca. 2220 ng/cm^2), it can be easily shown that the Ag^+ ion:StA ratio works out to nearly 45:1. This result was reproducible, and it was found that the mass uptake curves in separate runs agreed to within 5%. The QCM measurement indicates a high degree of overcompensation

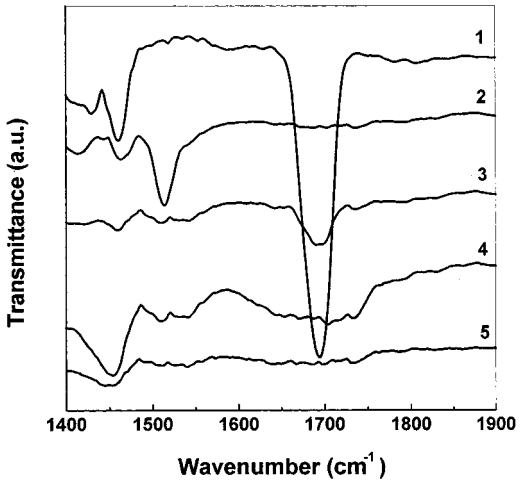

Figure 2. FTIR spectra recorded from a 500 Å thick StA film deposited on Si(111) substrate (curve 1); the StA film shown as curve 1 after incorporation of Ag^+ ions (curve 2); the StA film shown as curve 2 after reduction of Ag^+ ions (curve 3); the StA film shown as curve 3 after three cycles of Pd^{2+} ion exchange (curve 4) and reduction (curve 5).

of the charge in the StA film by the Ag^+ ions and is an aspect of the work which is not clear at the moment. However, It may be mentioned that such charge overcompensation is known to occur during complexation of macroions such as phosphotungstate anions[23] and DNA[24] with fatty amine Langmuir monolayers at the air−water interface and is also the mechanism by which layer-by-layer electrostatic assembly occurs on planar surfaces.[25]

After reduction of the silver stearate film by a 2 h hydrazine treatment, the QCM crystal was further immersed in $PdCl_2$ solution (10^{-4} M), and the Pd^{2+} QCM mass uptake recorded during this first cycle of immersion is shown in Figure 1. The final mass uptake during this cycle of ion exchange yielded a value of ca. 34 000 ng/cm^2 and results in a ca. 1:1.1 Pd^{2+}:Ag^+ weight ratio. In a similar manner, two more cycles of reduction and Pd^{2+} incorporation in the StA films were carried, out and the QCM mass uptake data for these cycles are also shown in Figure 1. In the second and third cycles of Pd^{2+} ion uptake, the final mass loadings were 19 250 and 9300 ng/cm^2 respectively. These values correspond to Ag^+:Pd^{2+} weight rations of 1:1.9 and 1:4.12 for cycles 2 and 3, respectively. Converting the mass uptake values into molar ratios yields an Ag^+:Pd^{2+} ratio of 1:1.8 over the entire cycle of ion exchange and reduction.

Figure 2 shows the FTIR spectra recorded in the range 1400−1900 cm^{-1} for a 500 Å thick StA film deposited on Si (111) wafer after various cycles of ion exchange and reduction. Curve 1 in the figure represents the spectrum recorded from the as-deposited StA film on Si. A number of prominent features are seen, the most germane to this study being the resonances at 1700 and 1470 cm^{-1}, which are assigned to the carbonyl stretch[20,26] and methylene scissoring[20,26−28] motions, respectively. We would like to point out that a single peak is seen at 1470 cm^{-1}, and this indicates that the hydrocarbon chains in the StA matrix are in a disordered state.[20,27,28] The FTIR spectrum recorded from the StA film after one cycle of Ag^+ incorporation is shown as curve 2 in Figure 2. It is observed that on formation of the silver salt of stearic acid, the carbonyl stretch frequency shifts from 1700 to ca. 1515 cm^{-1}, clearly indicating the binding of the Ag^+ ions with the carboxylate ions of StA. The shift in the carbonyl stretch frequency to lower wavenumbers followed by the disappearance of the 1700 cm^{-1} resonance is known to be a clear indicator of salt formation in such fatty acid films[20] and indicates in this case complete silver stearate salt formation.

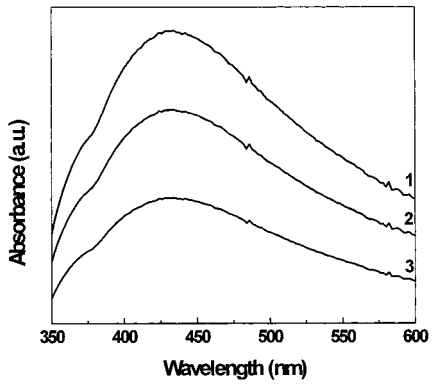

Figure 3. UV−vis spectra recorded from a 500 Å thick StA film on quartz after one cycle of Ag^+ ion exchange and reduction (curve 1); film shown as curve 1 after 1 cycle of Pd^{2+} incorporation followed by reduction (curve 2) and film shows as curve 2 after two more cycles of Pd^{2+} exchange and reduction (curve 3).

Reduction of the Ag^+ ions in the silver stearate film resulted in the FTIR spectrum shown as curve 3 in Figure 2. It is observed that the methylene scissoring band is considerably reduced in intensity, and the carbonyl stretch band now appears as a broad resonance centered at ca. 1700 cm^{-1}. The former result indicates that the hydrocarbon chains in the StA molecules are considerably disordered on formation of the silver nanoparticles. This may be a consequence of distortion to the bilayer structure of the lipid matrix induced by the presence of the silver nanoparticles and also due to surface coordination of stearic acid molecules to the silver particles generated in-situ. It is known that fatty acid molecules bind to colloidal silver[29] and, in the case of silver particles generated in the StA matrix, would lead to significant distortion to the lamellar, bilayer structure. As will be seen below, this inference is also in agreement with XRD data of the StA−silver nanofilm. The shift of the carbonyl stretch resonance to 1700 cm^{-1} is consistent with the regeneration of carboxylic acid groups on reduction of the Ag^+ ions. Curve 4 in Figure 2 represents the FTIR spectrum recorded from the film shown as curve 3 after three cycles of Pd^{2+} exchange. A very weak resonance at 1700 cm^{-1} is observed indicative of nearly complete formation of palladium stearate. A broad band at 1540 cm^{-1} is seen to arise due to the binding of Pd^{2+} ions to carboxylic acid groups. Curve 5 in Figure 2 represents the FTIR spectra recorded after reduction of the film shown in curve 4. The curve is essentially featureless indicative of complete formation of nanoparticles within the acid film. The absence of any band at 1700 cm^{-1} suggests the binding of free carboxylic acid groups with the reduced nanoparticles.

The reduction of Ag^+ and Pd^{2+} ions in the StA matrix is conveniently followed by UV−vis spectroscopy. While silver nanoparticles in solution show a strong and sharp resonance at ca. 400 nm due to excitation of surface plasmon oscillations,[30a] Pd nanoparticles exhibit a continuous absorption band in $\lambda =$ 300 nm.[31] Figure 3 shows the UV−vis spectrum recorded from a 500 Å thick StA film on a quartz substrate after the first cycle of Ag^+ ion exchange and reduction (curve 1). A fairly broad resonance centered at ca. 430 nm can be observed for this film and clearly shows the presence of silver nanoparticles in the StA matrix. The red shift in the wavelength at which maximum absorption occurs relative to that of particles in solution has been observed before in Langmuir−Blodgett films of silver nanoparticles formed by electrostatic assembly at the air−water interface[30b] as well as in nanocomposites of silver and octade-

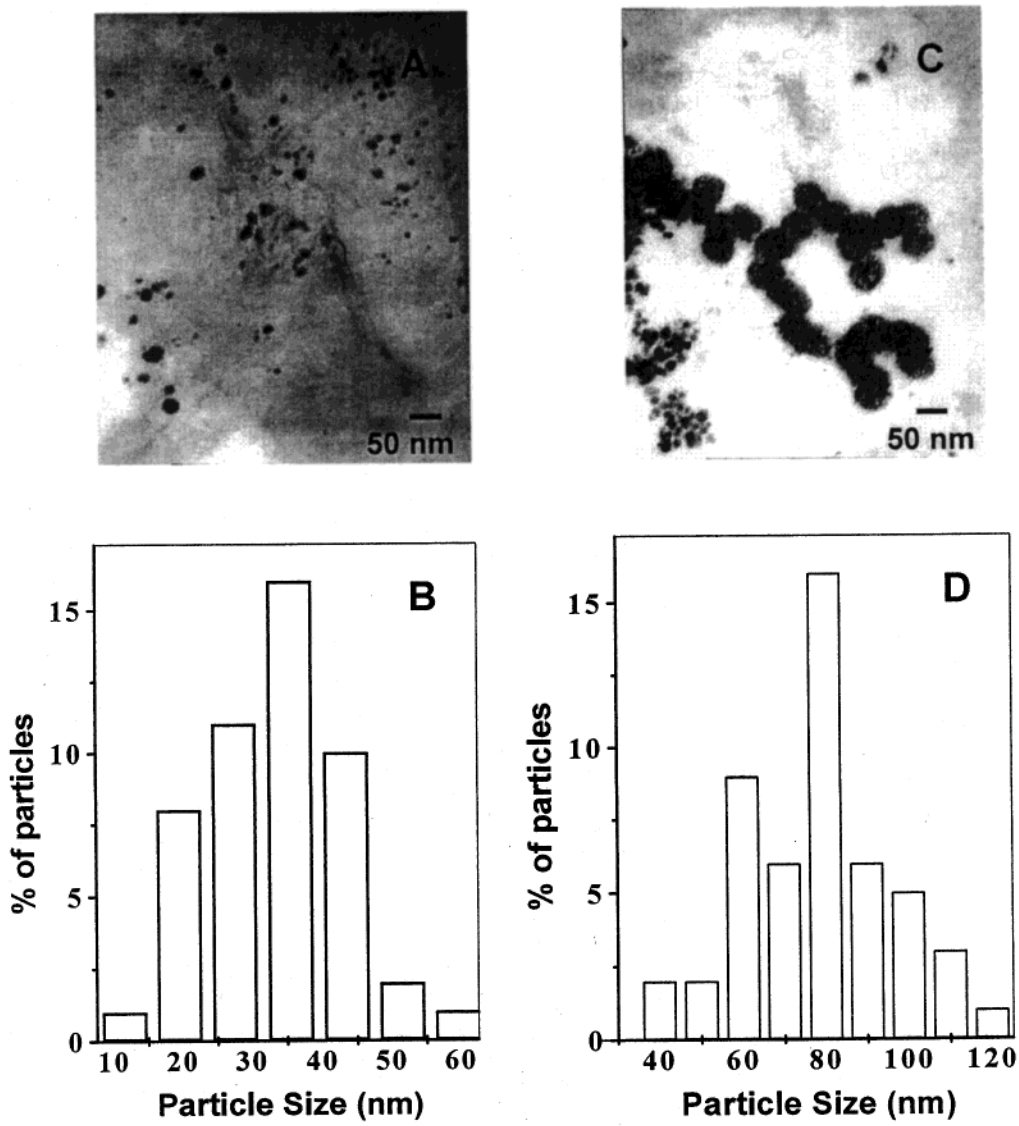

Figure 4. (A) TEM picture recorded from a 500 Å thick StA film after one cycle of Ag^+ ion incorporation and reduction. The lipid matrix was removed by soaking the StA−Ag nanocomposite film in chloroform for 15 min. (B) Particle size distribution histogram of the Ag nanoparticles shown in panel A. (C) TEM picture recorded from a 500 Å thick StA film after one cycle of Ag^+ ion incorporation and reduction followed by three cycles of Pd^{2+} incorporation and reduction. The lipid matrix was removed by soaking the StA−(Ag + Pd) nanocomposite film in chloroform for 15 min. (D) Particle size distribution histogram of the Ag−Pd nanoparticles shown in panel C.

cylamine formed by diffusion from solution.[30c] This red shift in the surface plasmon resonance wavelength is consistent with the Mie theory for the optical properties of colloidal silver[30a] and may be explained in terms of the increased refractive index of the medium experienced by the silver particles in the StA matrix when compared with silver particles in aqueous solution. The UV−vis spectrum recorded from the film shown as curve 1 in Figure 3 after a cycle of Pd^{2+} incorporation and reduction is represented by curve 2 in the figure. We would like to point out at this stage the importance of the UV−vis results. The reduction of the palladium ions in the StA/silver nanomatrix could proceed along two different pathways or a combination of the two. The first is that the palladium ions are reduced and the palladium atoms aggregate to form separate Pd nanoparticles. The second possibility is that the palladium ions get reduced on the surface of the silver nanoparticles already present in the StA matrix leading to a silver-core/palladium-shell structure. The latter route would lead to a damping of the dominant silver surface plasmon resonance by the surface layer of palladium as is clearly observed (compare curves 1 and 2, Figure 3). Two further cycles of Pd^{2+} incorporation and reduction resulted in the UV−vis spectrum shown as curve 3 in Figure 3. In this case as well, a distinct decrease in the absorbance is observed over the wavelength range spanning the plasmon excitations of silver. The UV−vis results thus clearly indicate reduction of at least a fraction of Pd^{2+} ions on the surface of the already present silver nanoparticles in the StA matrix to form a Ag-core/Pd-shell structure. However, the UV−vis evidence by itself is insufficient to unequivocally claim complete formation of Ag-core/Pd-shell structures within the lipid matrix. The growth of individual Pd nanoparticles in the lipid film after Pd^{2+} ion incorporation and reduction can take place due to the binding of carboxylate groups from the fatty acid film with Pd^{2+} ions. TEM measurements would help in ascertaining the relative contributions of the two Pd ion reduction pathways[32] and are discussed below.

A transmission electron micrograph recorded from a 500 Å thick StA film after one cycle of Ag^+ ion exchange and subsequent reduction with hydrazine is shown in Figure 4A. The StA matrix was removed from this composite film by soaking the film in chloroform for 15 min and carefully removing the TEM grid from the organic phase. A number of

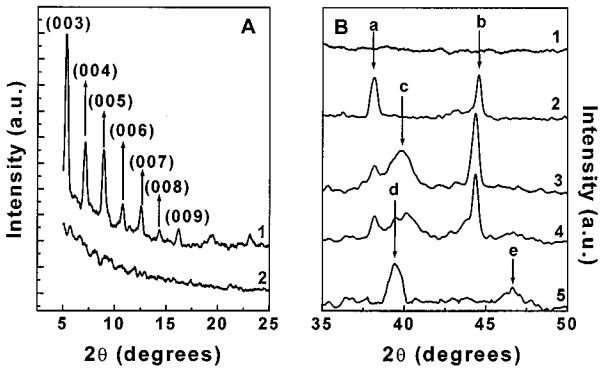

Figure 5. (A) XRD pattern recorded from a 500 Å thick StA film after incorporation of Ag^+ ions (curve 1) and the silver stearate film after reduction of the silver ions by hydrazine treatment to form silver nanoparticles (curve 2). The (00*l*) Bragg reflections are indexed in the figure. (B) XRD patterns in the range of the (111) Bragg reflections from Ag (feature a), Pd (feature c), and the Ag−Pd alloy (features d and e) recorded from a 500 Å thick StA film after immersion in Ag^+ ion solution (curve 1); film shown as curve 1 after reduction (curve 2); film shown as curve 2 after three cycles of Pd^{2+} incorporation and reduction (curve 3); film shown as curve 3 after heating a 100 °C for 6 h (curve 4); and film shown as curve 4 after additional heating at 100 °C for 12 h (curve 5).

well-dispersed particles can clearly be seen in the TEM picture with a fairly even size distribution. The particle size histogram for this micrograph is plotted in Figure 4B. This analysis yielded an average particle size of 33.2 ± 9.9 nm. Figure 4C shows the transmission electron micrograph recorded from a 500 Å thick StA film after one cycle of Ag^+ ion exchange and reduction and three cycles of Pd^{2+} ion exchange and reduction. From the particle size histogram for the micrograph shown in Figure 4C, an average particle size was determined to be 77.3 ± 18.1 nm (Figure 4D). An increase in the particle size after Pd^{2+} ion exchange and reduction clearly indicates formation of an Ag-core/Pd-shell structure, albeit in a fraction of the particles examined. A number of smaller particles in the size range 20−40 nm are also seen in the Figure 4C. These particles are clearly individual silver and freshly formed Pd nanoparticles.

Figure 5A shows the XRD patterns recorded from the StA film after the first cycle of Ag^+ ion incorporation (curve 1) and after reduction of the silver ions to form silver nanoparticles with one cycle of Pd^{2+} incorporation (curve 2). It is seen that the silver stearate film shows a *c*-axis oriented lamellar structure and a number of (00*l*) Bragg reflections are indexed in Figure 5A (curve 1). From the 2θ values of the seven Bragg reflections observed for this film, a *d*-spacing of 49 Å is calculated. This value is in good agreement with the expected *d*-spacing based on the length of the StA molecule and the size of the Ag^+ ion[33] and clearly shows the presence of an ordered, lamellar phase with the hydrocarbon chains of the StA molecules in the all-trans packing configuration. Please also note the characteristic odd−even intensity oscillations in the (00*l*) Bragg reflections from the silver stearate film (curve 1, Figure 5A). This intensity oscillation has been shown to be a consequence of lamellar ordering of films of fatty acid salts[33] and is, in some sense, a very sensitive indicator of the packing of the hydrocarbon chains in the film. On reduction of the silver ions to form silver nanoparticles followed by one cycle of Pd^{2+} incorporation, the lamellar ordering in the film vanishes, as evidenced by the disappearance of the (00*l*) Bragg reflections (curve 2, Figure 5A). The fact that incorporation of Pd^{2+} ions after the reduction process does not lead to restoration of lamellar order in the films indicates that the distortion to the bilayer structure on formation of the silver nanoparticles is quite large and suggests a significant density of large sized silver particles in the film.

Figure 5B shows XRD patterns recorded from a 500 Å thick StA film after the first cycle of Ag^+ incorporation (curve 1), the film shown as curve 1 after reduction of the silver ions (curve 2), the film shown as curve 2 after three cycles of Pd^{2+} incorporation and reduction in the films (curve 3), film shown as curve 3 after heating at 100 °C for 6 h (curve 4), and film shown as curve 4 after additional heating at 100 °C for 12 h (curve 5). A number of features labeled a−e can be seen in the figure and are located at 2θ values of 38.2°, 44.1° 40.1°, 39.4°, and 46.8°, respectively. While the silver stearate film is essentially featureless in the 2θ range 35−55° (Figure 5B, curve 1), reduction of the silver ions by hydrazine treatment leads to growth of the (111) Bragg reflection at a 2θ value of 38.2° from the silver nanoparticles generated in-situ (Figure 5B, curve 2, feature a). The XRD pattern recorded from the reduced silver stearate film after three cycles of Pd^{2+} ion incorporation and reduction is represented as curve 3, Figure 5B. An additional peak at a 2θ value of 40.1° is clearly seen in this diffraction pattern (feature c) and arises due to the (111) Bragg reflection from the Pd particles grown in the StA matrix. The StA/(silver + palladium) nanofilm was heated at 100 °C for 6 h, and the XRD pattern obtained after this thermal treatment is represented by curve 4, Figure 5B. Two new Bragg reflections at 2θ values of 39.4° and 46.8° are observed from this film and are assigned to the (111) and (200) reflections, respectively, from the Ag_xPd_{1-x} alloy phase. The intensities of these reflections are weak and alloy formation is not complete which is indicated by the continued presence of Ag (111) and Pd(111) peaks in the diffraction pattern (features a and c, respectively). After formation of the Ag−Pd alloy phase, the film shown as curve 4 in Figure 5B was heated for a further 12 h at 100 °C to see whether either the silver or palladium particles could be consumed completely in the alloy phase. The XRD pattern obtained from this film is shown in Figure 5B as curve 5. It is interesting to note the complete disappearance of features a and c that correspond to Ag (111) and Pd (111) Bragg reflections. Apparently, further heat treatment to the film has resulted in the complete formation of the Ag−Pd solid solution at 100° C, such alloy formation normally reported to take place at temperatures above 1000° C in the case of bulk Ag−Pd system[34] and above200 °C in the case of epitaxial Ag/Pd superlattices.[35a] These peaks agree well with those reported in the literature for the alloy phase.[35b] Considering Vegard's law behavior for the Ag−Pd system,[17a] the composition of the solid solution can be calculated from the position of the Ag_xPd_{1-x} (111) peak (39.4°) to be $Ag_{0.4}Pd_{0.6}$. This result is in good agreement with the Pd:Ag ratio of ca. 1.8:1 calculated from the QCM data (Figure 1). Prior to the thermal treatment at 100° C, we had measured the XRD spectrum from the StA/(silver + palladium) nanofilm heated at 50° C and 75 °C for 6 h and did not notice any changes associated with the formation of an alloy phase. This result suggests that the high surface free energy of the metal in nanoparticle form is, to a large extent, responsible for this considerable lowering of the annealing temperature. Efforts are underway to control the size of the silver and palladium nanoparticles synthesized by the ion-exchange route presented in this paper and seek a possible correlation between particle size and alloying temperature. The role played by the StA matrix on the alloying process is another aspect that requires further investigation.

In conclusion, the formation of Ag and Pd nanoparticles in thermally evaporated stearic acid films by a process of ion

exchange and reduction has been demonstrated. The silver and palladium particles could be grown simultaneously in the fatty acid matrix resulting in both individual Ag and Pd nanoparticles as well as particles in the Ag-core/Pd-shell structure. A low-temperature heat treatment of the Ag/Pd nanoparticle film at 100 °C resulted in the formation of an Ag−Pd alloy phase within the fatty acid matrix. This is a salient result of the investigation, such bimetallic formation normally reported to occur in colloidal solutions.[35b] Efforts are underway to control the size of the nanoparticles grown by this route and investigating other noble metal bimetallic structures.

Acknowledgment. One of us, A.K., thanks the Council of Scientific and Industrial Research (CSIR), Government of India for a research fellowship. This work was partially supported by a grant from the Indo-French Centre for the Promotion of Advanced Scientific Research (IFCPAR), New Delhi, and that is gratefully acknowledged. The authors gratefully acknowledge the TEM assistance rendered by Ms. Renu Parischa, Materials Chemistry Division, N.C.L Pune.

References and Notes

(1) Aliviasatos, A. P. *Science* **1996**, *271*, 933.
(2) Beecoft, L. L.; Ober, C. K. *Chem. Mater*. **1997**, *9*, 1302.
(3) Justus, B. L.; Tonnucci, R. J.; Berry, A. D. *Appl. Phys. Lett.* **1992**, *61*, 3151.
(4) Wang, Y.; Herron, N. *J. Phys. Chem.* **1988**, *92*, 4988.
(5) Zhao, X. K.; Barai, S.; Rolandi, R.; Fendler, J. H. *J. Am. Chem. Soc*. **1988**, *110*, 1012.
(6) Dresco, P. A.; Zaitsev, V. S.; Gambino, R. J.; Chu, B. *Langmuir* **1999**, *15*, 1945.
(7) Garcia, M. E.; Baker, L. A.; Crooks, R. M. *Anal. Chem.* **1999**, *71*, 256.
(8) Patil, V.; Mayya, K. S.; Sastry, M. *J. Mater. Sci. Lett.* **1997**, *16*, 899.
(9) (a) Shenton, W.; Pum, D.; Sleytr, U. B.; Mann, S. Nature **1997**, 389, 585. (b) Sleytr, U. B.; Messner, P.; Pum, D.; Sara, M. *Angew. Chem., Int. Ed. Engl*. **1999**, *38*, 1034.
(10) Shenton, W.; Douglas, T.; Young, M.; Stubbs, G.; Mann, S. *Adv. Mater*. **1999**, *11*, 253.
(11) (a) Elliot, D. J.; Furlong, D. N.; Gegenbach, T. R.; Grieser, F.; Urquhart, R. S.; Hoffman, C. L.; Rabolt, J. F. *Colloid Surf. A.* **1995**, *103*, 207. (b) Taylor, D. M.; Lambi, J. N. *Thin Solid Films* **1994**, *243*, 384. (c) Paranjape, D. V.; Sastry, M.; Ganguly, P. *Appl. Phys. Lett.* **1993**, *63*, 18. (d) Amm, D. T.; Johnson, D. J.; Laursen, Y. Gupta, S. K. *Appl. Phys. Lett.* **1992**,*61*, 522.
(12) Toshima, N.; Harada, M.; Yonezawa, T.; Kushihashi, K.; Asakura, K. *J. Phys. Chem* **1991**, *95*, 7448.
(13) Torigoe, K.; Nakajima, Y.; Esumi, K. *J. Phys. Chem.* **1993**, *97*, 8304.
(14) Liz-marzan, L. M.; Philipse, A. P. *J. Phys. Chem.* **1995**, *99*, 15120.
(15) (a) Toshima, N.; Harada, M.; Yamazaki, Y.; Asakura, K. *J. Phys. Chem*. **1992**, *96*, 9927. (b) Mizukoshi, Y.; Yamamoto, T.; Nagata, Y.; Okitsu, K.; Maeda, Y. *J. Phys. Chem. B.* **1997**, *101*, 7033.
(16) (a) Aihara, N.; Torigoe, K.; Esumi, K. *Langmuir* **1998**, *14*, 4945. (b) Itakura, T.; Torigoe, K.; Esumi, K. *Langmuir* **1995**, *11*, 4129.
(17) (a) Vasan, H.; Rao, C. N. R. *J. Mater. Chem*. **1995**, *5*, 1755. (b) Venezia, A.; Liotta, L.; Deganello, G.; Schay. Z.; Guczi, L. *J. Catal*. **1999**, *182*, 449.
(18) Torigoe, K.; Esumi, K. *Langmuir* **1993**, *9*, 1664.
(19) Michaelis, M.; Henglein, A. *J. Phys. Chem*. **1994**, *98*, 6212.
(20) Ganguly, P.; Pal, S.; Sastry, M.; Shashikala, M. N. *Langmuir* **1995**, *11*, 1078.
(21) Sauerbrey, G. *Z. Phys. (Munich)* **1959**, *155*, 206.
(22) Patil, V.; Sastry, M. *Langmuir* **2000**, *16*, 2207.
(23) Cuvillier, N.; Rondelez, F. *Thin Solid Films* **1998**, *19*, 327.
(24) Sastry, M.; Ramakrishnan, V.; Pattarkine, M.; Ganesh, K. N. *Langmuir* **2000**, *16*, 9142.
(25) Decher, G. *Science* **1997**, *277*, 1232.
(26) Rabolt, J. F.; Burns, F. C.; Schlotter, N. E.; Swalen, J. D. *J. Chem. Phys.* **1983**, *78*, 946.
(27) Snyder, R. G. *J. Mol. Spectrosc.* **1961**, *7*, 116.
(28) Lala, N.; Sastry, M. *Phys. Chem. Chem. Phys.* **2000**, *2*, 2461.
(29) Patil, V.; Mayya, K. S.; Pradhan, S. D.; Sastry, M. *J. Am. Chem. Soc.* **1997**, *119*, 9281
(30) (a) Henglein, A. *J. Phys. Chem.* **1993**, *97*, 5457. (b) Sastry, M.; Mayya, K. S.; Paranjape, D. V.; Hegde, S. G. *J. Phys. Chem. B.* **1997**, *101*, 4954. (c) Sastry, M.; Patil, V.; Sainkar, S. R. *J. Phys. Chem. B* **1998**, *102*, 1404.
(31) Creighton, J.; Eadon, D. *J. Chem. Soc., Faraday Trans.* **1991**, *87*, 3881.
(32) Henglein, A. *J. Phys. Chem. B.* **2000**, *104*, 6683.
(33) Ganguly, P. Paranjape, D. V.; Patil, K. R.; Chaudhari, S. K. *Langmuir* **1992**,*8*, 2365
(34) Massalki, T. B.; Okamoto, H.; Subramanian, P. R. *Binary Alloy Phase Diagrams*, 2nd ed.; ASM International: Metals Park: OH, 1990.
(35) (a) Temst, K.; Van Bael, M. J.; Van Haesendonck, C.; Bryseraede, Y.; de Groot, D. G.; Koman, N.; Griessen, R. *Thin Solid Films* **1999**, *342*, 174. (b) Silvert, P. Y.; Vijayakrishnan, V.; Vibert, P.; Herrera-Urbina, R.; Elhsissen, K. *Nanostruct. Mater*. **1996**, *7*, 611.